JOURNAL OF PROPULSION AND POWER
Vol. 11, No. 6, November–December 1995

Structure of a Swirl-Stabilized Spray Flame Relevant to Gas Turbine and Furnaces

Kyeong Lee* and Behrouz Chehroudi†
University of Illinois at Chicago, Chicago, Illinois 60680

To investigate the structure of a hollow-cone spray flame similar to those occurring in the primary zone of gas-turbine combustors or within furnaces, a swirl-stabilized combustor was used. A kerosene spray was produced by a simplex atomizer with a nominal included-cone-angle of 30 deg. Swirling air had a calculated swirl number of 0.36 and was produced by a swirl plate having an exit air velocity vector of 30 deg with respect to the chamber axis. A phase Doppler particle analyzer was used to measure drop size; mean and root mean square (rms) values of axial, radial, and tangential components; and drop velocity and size probability distribution functions (PDFs) at five different axial positions from the nozzle. A mean spray flame structure and terminology are proposed. It is found that a large portion of the drop flowfield within this spray flame is dominated by radial and axial components of the velocity vector. It appears that sufficiently away from the nozzle the direction of the mean droplet velocity vector is primarily established by the design of the swirl plate. Based on the bimodal behavior of drop axial velocity PDF, pulsation of the central recirculation zone is proposed and the extent of its effect on the droplet field is investigated. The rms of droplet flowfield is not isotropic in this spray flame. At each axial position, axial rms has the highest value among the three components and occurs near the maximum temperature point. Moving away from the nozzle near and along the locus of maximum mean temperature, strong preferential evaporation and/or burning of small drops drastically affect the shape of the size PDFs by progressively shifting its profile into larger size ranges.

Introduction

MANY practical devices such as diesel, gas turbine, and rocket engines use liquid fuel spray in their combustion chamber to produce power for a variety of applications. Furnaces, oil burners, and incinerators are other examples in which liquid fuel spray is used. In the aforementioned applications the liquid fuel must be atomized to droplets by appropriately designed fuel nozzles. Atomizers are of different designs for different applications. Also, the combustor shape, flowfield, and thermodynamic conditions are drastically different for different cases. Hence, a universal treatment and comprehensive knowledge on spray combustion are still lacking in the literature. For these reasons detailed experimental, theoretical, and numerical investigations of each case are needed for a complete understanding of the important processes in spray combustion to aid in designing more fuel efficient and less environmentally destructive power generation/conversion devices.

Many systematic experimental efforts on swirl-stabilized model combustors simulating spray combustion in furnaces, oil burners, and gas-turbine engines are available in the literature.[1-12] A detailed comparison and generalization of all the conclusions reached in these works are difficult because different fuel nozzles, fuels, chamber geometries, and operating conditions are used.

This article concentrates on the experimental investigation of hollow-cone spray flames similar to those occurring in the primary zone of gas-turbine combustion chambers or liquid-fuel-burned furnaces. To achieve this, a swirl-stabilized flame combustor was constructed to simulate liquid fuel combustion in these devices. This is an important first step towards a more realistic condition, e.g., higher chamber pressures and/or initial temperature in gas-turbine research. The objective of this article is to report our findings and results on a droplet flowfield from a spray flame in a single-model swirl-stabilized combustor.

Received April 8, 1994; revision received Sept. 28, 1994; accepted for publication Feb. 13, 1995.

*Graduate Student, Department of Mechanical Engineering; currently at GMI Engineering and Management Institute, Flint, MI 45504.

†Assistant Professor, Engine Laboratory, Department of Mechanical Engineering; currently at GMI Engineering and Management Institute, Flint, MI 45504.

Experimental Setup and Instrumentation

Swirl-Stabilized Combustor

Schematic diagrams of the experimental rig and the combustor used in this study can be found in Fig. 1. A circular cross-sectional stainless-steel outer pipe 265 mm in diameter and 813 mm in length is vertically positioned under a labo-

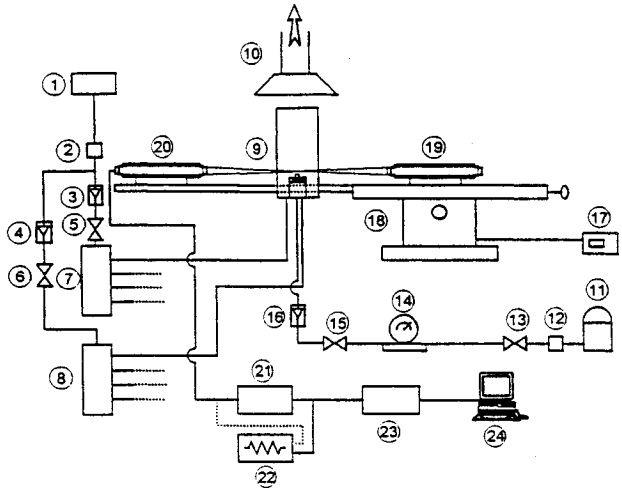

Fig. 1 Components of the experimental setup. 1. Compressor, 2. air filter/regulator, 3. rotameter, 4. rotameter, 5. valve, 6. valve, 7. dilution air tank, 8. swirl air tank, 9. combustor, 10. stack, 11. fuel tank, 12. fuel filter, 13. valve, 14. fuel pump, 15. valve, 16. rotameter, 17. digital readout, 18. three-dimensional traverse table, 19. PDPA transmitter, 20. PDPA receiver, 21. high-low bandpass filter, 22. oscilloscope, 23. A/D converter, and 24. computer.

ratory exhaust suction system. An inner pipe, concentric with the outer pipe, 102 mm in diameter and 254 mm in length, is installed on a 38-mm-thick lower end plate. The main air from the compressor goes through a regulator/filter assembly and then is divided into two branches, one for dilution air and the other for swirl air. Air in each branch passes through a rotameter (Dwyer, model VFC-122-BV with ±2.5% of the reading accuracy) and a valve (NIBCO, T-275-B) before going into a large tank. For uniform air distribution, air from each tank is directed to the combustor by four pipes. Each pipe ends in a specially designed distributor for even spreading of the air in all directions within the combustor. A set of honeycomb is installed at an axial position of 101 mm from the end plate to allow uniform air distribution inside the combustor. Fuel is supplied through filters from a tank and is pumped by a fuel pump (Suntec. model A2VA-7016) into an on-axis vertically adjustable tube after passing through a fuel rotameter (Brooks, model 1110-R-2-15-B). Sunnyside K-1 kerosene was used for all results reported here. Ignition is achieved via a small side-wall opening with a propane torch.

A Delavan (model 0.75-30A) industrial-type pressure-swirl nozzle is used to generate an axisymmetric spray. The nozzle produces a typical hollow-cone spray with a nominal total spray angle of 30 deg at a rated flow rate of 48.1 ± 0.99 cc/min (fuel density of 0.8 g/cc) and a constant injection pressure of 100 psi. Liquid fuel within the nozzle flows tangentially into a swirl chamber at high pressure and passes through a diffuser to a circular exit–orifice. The spray droplets swirl in a clockwise direction.

An air swirl plate 102 mm in diameter and 19 mm in thickness is installed at the top end and the same level as the upper edge of the swirl (i.e., inner) pipe. The nozzle tip protrudes axially by 6 mm from the upper face of the swirl plate. This arrangement was found to produce the most stable flame condition in our setup. Ten tangentially arranged and equally spaced radial slots 33 mm in length and 6 mm in width on the face of the swirl plate produced clockwise swirling airflow in the combustor. The swirl exit velocity vector from each slot is designed to be at a 30-deg angle with respect to the combustor axis. This design simulates a class of simple swirlers used in some swirl-stabilized combustors such as oil burners and furnaces. A swirl number of 0.36 was obtained by calculation.[13]

Phase Doppler Particle Analyzer (PDPA)

A single-component PDPA is used to obtain simultaneous droplet size and velocity measurements.[14] The optical system consists of a transmitter and a receiver, model nos. XMT-1100-4S and RCV-2100, respectively. The transmitter contains a spectraphysics model SP-106, 10-mW, polarized He-Ne laser. Both components are mounted on a three-dimensional traversing table with a one-digital readout for each direction. An output lens of 495 mm focal length (f.l.) with f/no. 4.7 and a collimating lens of 300 mm f.l. are used for the transmitting optics, and an output lens of 495 mm f.l. with f/no. 7 and a collimating lens are installed behind a slit for receiving optics. Spatial filter in the receiver has a slit 100 m wide by 1 mm long. At most of the measurement points, 12,000 data points were set by the PDPA software. In the dilute spray region, data points were collected with two limitations of a maximum data-collection time of 10 min and total data points of 3200. Statistical uncertainties were estimated to be about ±3% and ±6% for the mean and rms of velocity fluctuations, respectively. Drop sizes were measured simultaneously with only an axial drop velocity component, and the drop size measurement option of the PDPA was turned off for radial and tangential component measurements.

Results and Discussion

As fuel atomizer parameters and swirl plate geometry are fixed, dilution and swirl airflow rates become important variables for flame stability in our facility. Previous works in our engine laboratory defined, in our combustor, a region within which a stable flame could exist as a function of swirl and dilution airflow rates.[15–17] They performed all their experiments at swirl and dilution airflow rates of 3.69 and 1.55 kg/min, respectively, being within the stable region. Flame stability was judged by observation and measurements of the average flame tip height as a function of the swirl airflow rate at a dilution airflow rate of 1.55 kg/min. In this work, the stable flame region was also investigated by observation of the flame configuration and found to be in agreement with previous results referenced previously. Thus, the combination of 3.69/1.55 kg/min was used for all results presented here.

Schematic Diagram of the Flame Mean Structure

Figure 2 exhibits a schematic diagram defining the mean structure of the swirl-stabilized spray flame used in this study. This structure was constructed based on the flame photography and PDPA measurements conducted by Lee[18] and previous works in our engine laboratory. Figure 2 introduces a consistent terminology used hereafter. The spray sheath (SSH) is the region within which droplet measurements are possible by PDPA. This is determined from the data presented in Fig. 3. The turbulent flame-brush (TFB) zone outer boundary is defined from tracing the contours of the outer boundary of this "visible" zone in photographs taken at different exposure times and aperture f/nos. (see Refs. 17 and 18). Since the maximum radially reachable position of the imaged turbulent flame varies depending on the camera exposure time, a contour obtained at an optimum exposure time of 1/15 s at f/8 was chosen after extensive study. In Fig. 2, the flame-brush zone inner boundary at each fixed distance from the nozzle is defined as the radial position where the measured mean temperature radial profile reaches its maximum value. This, as shown later in Fig. 3, happens to occur very near the first radial position where measurement of the mean axial drop velocity is possible and practical by the PDPA at each axial position. The preheat/reaction (P/R) zone is a region between the outer boundaries of the TFB and SSH zones as shown in Fig. 2. Also, the burned-gases (BG) zone is shown in this figure. The internal recirculation zone is a typical feature of a swirl-stabilized hollow-cone spray flame.[19] The flame is stabilized by recirculation of hot burned gases near the atomizer providing a continuous ignition source. Existence of this recirculation zone in our spray was confirmed in previous works performed in our engine laboratory.[16,18,20,21] They obtained both negative drop and gas velocity distributions in the central region of spray under a nonburning condition. The aforementioned terminology is used for the following discussion of our results.

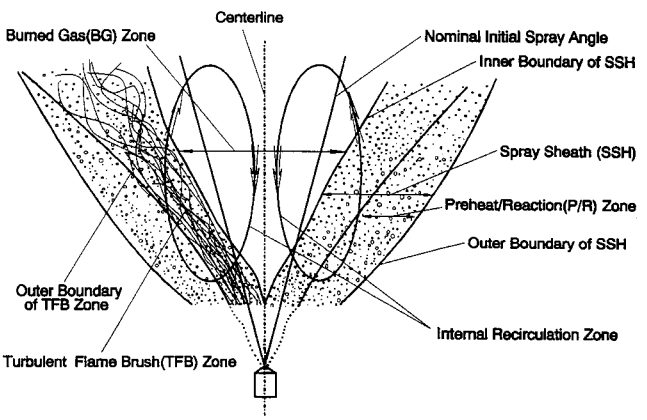

Fig. 2 Schematic diagram for the mean structure of the swirl-stabilized spray flame investigated in this study. This diagram also defines the proposed terminology used in this article.

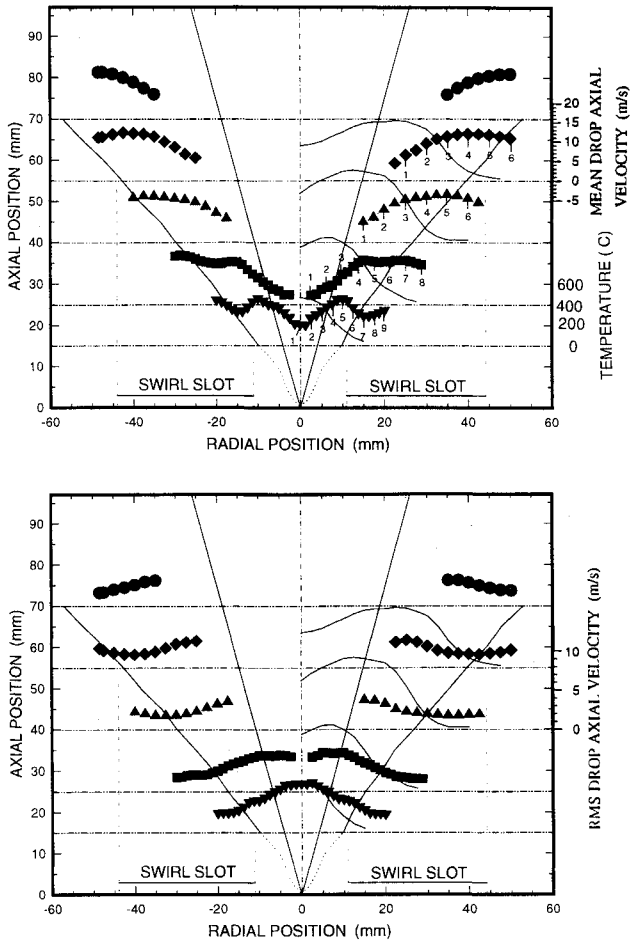

Fig. 3 Offset plot of the average temperature, mean and rms of the drop axial velocity fluctuations at five different axial positions.

Parametric Study

A parametric study on instrument variables was performed to determine "optimum" choices of instrument variables, i.e., shift velocity in this case.[17,22–25] The optimum velocity shift of the PDPA for experiments conducted here was set to achieve the least sensitivity of the measured quantities to changes in this variable. Our purpose was to choose optimum instrument-variable operating conditions based on some repeatable logic. The proposed choice of these variables based on maximizing the drop volume flux at each measurement location by McDonell and Samuelsen[23] may not work, as it does not reach a maximum value at each position.[24] For further discussion and justification refer to Ref. 17. Five test points for the radial and four for the tangential velocity components were selected, considering the dense and dilute regions of the spray. As a result, a velocity shift of 35 m/s was chosen as an optimum value for drop radial and tangential velocity component measurements. Also, everything else being ideal, a successful measurement of drop velocity through counter-type processing (which requires the existence of a preset number of zero-crossed signal cycles), of the burst signal depends on the direction at which a particle travels through the measurement volume relative to the fringes. This dependence of velocity measurability on the particle travel direction is known as the "fringe bias" (see Ref. 26). The angle between the trajectory of a particle producing a sufficient number of fringes and a line perpendicular to the plane of the fringes (i.e., the acceptance cone angle) was calculated to ensure maximum particle acceptance probability. The previously mentioned choice of velocity shift value was confirmed by this calculation to provide a fairly wide and adequate acceptance cone-angle for droplets in this study.

In the meantime, parametric study for the effects of shift velocity and photomultiplier (PM) tube voltage on drop axial velocity component was investigated in previous works.[15] The velocity shift of 20 m/s and the PM-tube voltage of 350 V dc were chosen as a set of optimum instrument variable values for the measurement of the axial velocity component. The PM-tube voltage of 350 V dc was also found to be appropriate in this study and produced low data rejection rate values. Thus, this work employs a velocity shift of 20 m/s for only the axial drop velocity component and a PM-tube voltage of 350 V dc for measurements of all drop velocity components.

Droplet Flowfield

Figure 3 shows radial offset profiles for the mean and rms of drop axial velocity fluctuations measured at five axial positions of Z = 15, 25, 40, 55, and 70 mm. The dash–dot–dot horizontal lines in this figure exhibit mean and rms base levels of 0 m/s, one for each axial position and its profile. Two inner upward-diverging lines exhibit the extent of the isothermal spray if traveled at a nominal initial spray angle of 30 deg. The two outer diverging curves exhibit the outer boundary of the visible TFB zone taken from long-exposure photographs explained earlier. The lower part of this outer boundary below Z = 15 mm is presented as dotted curves (deduced from photographs in Ref. 18) since no velocity measurements were performed there. Up to an axial position of about Z = 10 mm, liquid fuel was clearly visible with no sign of shining flame.

At Z = 15 mm, a double-humped profile is clearly exhibited in Fig. 3. This shape spreads out with axial distance from the nozzle and finally resembles a section of a parabolic curve in each side of the centerline. It is noted that minimum values of the mean drop axial velocity profiles at Z = 15 and 25 mm are located near the central region. The "average" temperature was measured by thermocouple and discussed in detail by Ghaffarpour and Chehroudi.[17] Here, temperature profiles are shown in the right half of Fig. 3. The left half is fairly similar to the right one. For the purpose of this article the location of the maximum temperature and its general shape at each axial position are of prime interest. At each axial position, the average temperature gradually increased from the outer boundary of the P/R zone to a maximum at the inner boundary of the TFB zone. It then decreased to a local minimum at the centerline. This latter decline of the temperature is nonexistent at Z = 15 mm. Note that the TFB inner boundary was defined by the radial location of the maximum temperature. Hence, at each side of the centerline, the absolute minimum point for the mean drop axial velocity profile occurred where the maximum mean temperature existed at any axial position. The peak points in the mean axial velocity profile seem to fall near the TFB outer boundary at almost all axial positions. The second rise-up at the extreme ends of the profiles near the nozzle (at Z = 15 and 25 mm) is believed to be due to the introduction of the air jets from the swirl plate. The profiles for the rms of drop axial velocity fluctuations in Fig. 3 show their peak values near the common boundary between the BG and TFB zones. Also, this peak point almost coincides with the maximum point of the mean temperature radial profile. This trend is attributed to strong interactions between the droplets and flame and the BG reverse-flow in the internal recirculation zone. Meanwhile, this maximum value of the rms drop axial velocity fluctuations is highest at the nozzle exit and decreases with an increase in axial position.

Figure 4 presents radial profiles of the mean and rms of drop radial velocity fluctuations. The positive value for radial velocity means outward motion of drops from the centerline. Note that the magnitude of mean drop radial velocity is positive at all axial positions. This, however, doesn't mean that radial velocities of all droplets passing through the measurement volume are positive, i.e., outward. A double-humped

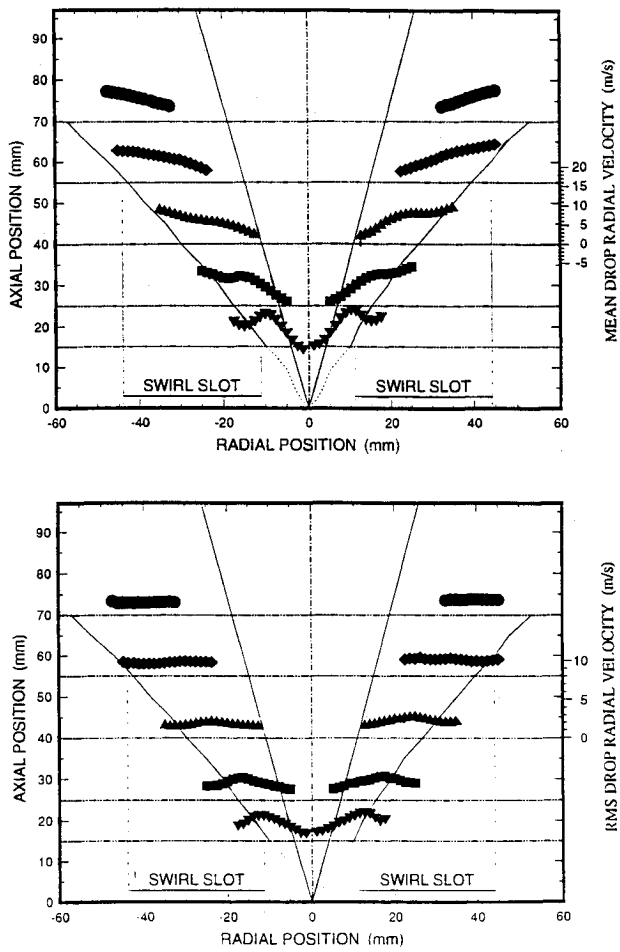

Fig. 4 Offset plot of the mean and rms of the drop radial velocity fluctuations at five different axial positions.

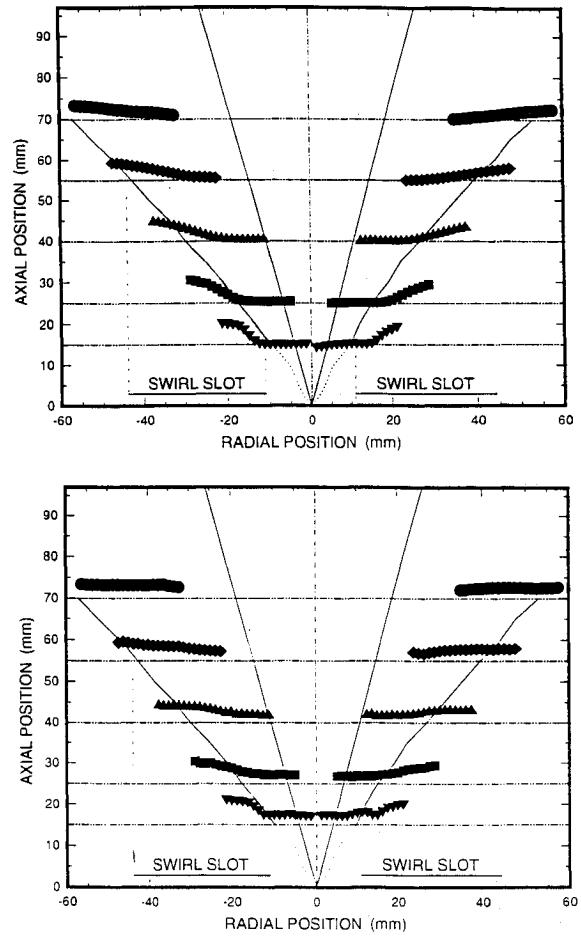

Fig. 5 Offset plot of the mean and rms of the drop tangential velocity fluctuations at five different axial positions. Scales same as Fig. 4.

feature appears near the nozzle that gradually spreads out with an increase in axial position. Further observations show that the absolute minimum points of the mean drop radial velocity profiles are located close to the inner boundary of the TFB zone, having near-zero values close to the nozzle ($Z = 15$ and 25 mm). On the other hand, inside the TFB zone, profiles sharply increase toward the outer boundary of this zone. This increase continues into the droplet-air mixing layer region, i.e., P/R zone, but with a milder slope. An exception to this exists at $Z = 15$ mm where it is influenced by the swirling flow. The rms profile of drop radial velocity in Fig. 4 exhibits high turbulent intensity near the outer boundary of the TFB zone. The rms value near this boundary decays as one moves away from the nozzle. Meanwhile, the minimum rmss are located near the inner boundary of the TFB zone where the maximum mean temperature exists. These trends exhibit a clear contrast to the results for rms of axial velocity fluctuations presented in Fig. 3.

Figure 5 indicates radial profiles of the mean and the rms of drop tangential velocity fluctuations. Up to $Z = 25$ mm from the nozzle, tangential velocities are almost zero inside the TFB zone, and then gradually increase with an increase in radial distance. Particularly at $Z = 15$ mm, tangential drop velocities start to increase at about the inner edge of the swirl slot and have their maximum values at the outer boundary of the P/R (or SSH) zone. These maximum values decrease moving away from the nozzle. Therefore, it is obvious that the swirling air governs the mean drop tangential velocity component and its effects decrease with an increase in axial position. Finally, it can be interpreted that in this spray flame droplet flowfield in the TFB zone is mainly governed by the axial and radial velocity components. The rms profiles of drop

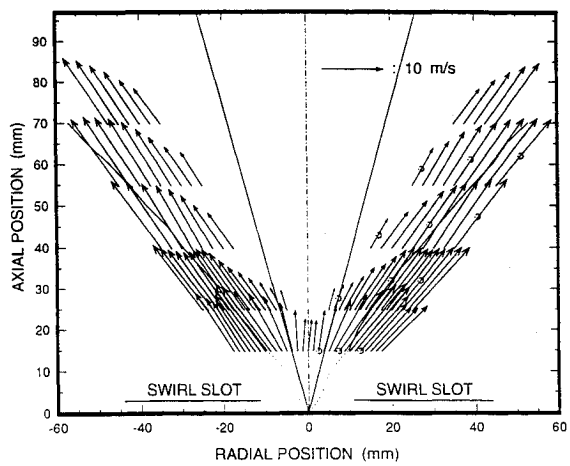

Fig. 6 Offset plot of the mean drop velocity vector in the vertical plane passing through the chamber centerline at five different axial positions.

tangential velocity fluctuations in Fig. 5 show that in the TFB zone, the rms values are nearly uniform, with the exception of a slight increase observed on the left side of the centerline, due to some asymmetry. Within the P/R zone, however, the rms values increase with radial distance. In the meantime, the overall mean and rms values at each axial position decay with distance from the nozzle.

Figure 6 exhibits vector plots of the mean droplet velocities at five axial positions in a vertical plane. It is interesting to note the change in magnitude of mean drop velocity vectors along mean drop-trajectories near the inner and outer bound-

aries of the TFB zone. Along a drop-trajectory near the inner boundary, the magnitude of the velocity vector suddenly decreases from $Z = 15$ to 25 mm (deceleration) due to effects of the reversed gas-flow established by the internal recirculation zone. It then gradually increases with axial position and almost recovers its initial magnitude at $Z = 55$ mm. Along a mean drop-trajectory near the outer boundary of the TFB zone, however, the velocity vector nearly preserves its initial magnitude up to the axial position of $Z = 55$ mm. Meanwhile, along a mean drop-trajectory within the TFB zone, it can be observed that the radial component is relatively increased moving away from the nozzle. This can be interpreted as radial diffusion of the flame zone. Note that, at each axial position, the radial position of the maximum velocity vector occurs inside and very near the outer boundary of the TFB zone. At $Z = 15$ the velocity–vector radial profile within the P/R zone exhibits a sharp decrease followed by a rise towards its outer boundary. The final rise is due to interaction of the slot jet from the swirl plate and fuel droplets. Similar, but weaker behavior is also observed at $Z = 25$ mm. The angles between the vectors and a vertical line in Fig. 6 are measured within 30–35 deg at all distances from the nozzle and at radial positions larger than about 8 mm (see Lee[18]). Close to the geometric axis and at $Z = 15$ and 25 mm, however, it increases from a near-zero value to 30–35 deg with radial position. It appears that sufficiently away from the nozzle this mean angle is established by the swirl plate slot-jet exit velocity vector of 30 deg.

Drop Size

Spatially resolved profiles of drop sizes are highly influenced by the gas flow pattern within the combustor. These profiles along with others establish significant characteristics of spray combustion. The Sauter mean diameter (SMD) physically represents the centroid drop-diameter for the surface area of the polydispersed spray, i.e., the diameter around which the spray surface area is centered. For this reason, SMD is also called surface area-weighted diameter. Thus, large drops have a stronger influence on SMD values.

Figure 7 represents the radial profile of the SMD measured at five axial positions of $Z = 15$, 25, 40, 55, and 70 mm. The dash–dot–dot horizontal line at each axial position downstream of the nozzle exit-plane exhibits a base SMD level of 20 μm. The SMD profiles show a broadening of spray with axial position as expected. At $Z = 15$ and 25 mm, the double-humped profile explicitly appears, being a typical pattern for hollow-cone spray flames. It is of interest that at $Z = 15$ and 25 mm, the radial positions of the local maximum points of SMD profile nearly coincide with the outer boundary of TFB zone. Downstream of $Z = 25$ mm, however, no local maximum exists and the absolute maximum point of the SMD

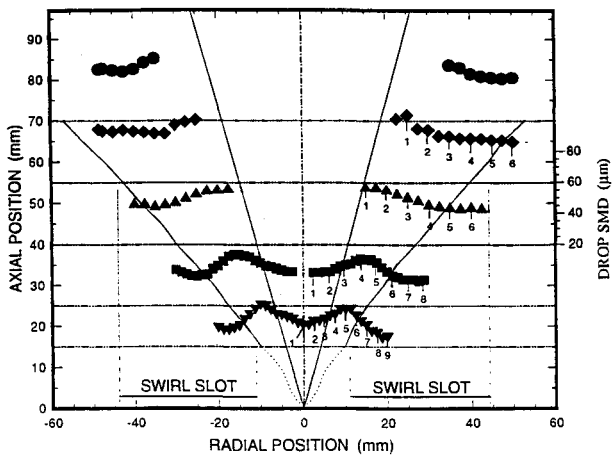

Fig. 7 Offset plot of the SMD at five different axial positions.

profile is positioned near the inner boundary of the TFB zone (or SSH zone). As mentioned before, the innermost radial position at which mean drop size and velocity measurements were possible located itself at or near the maximum of the mean radial temperature profiles. Also note that the hottest axial position is somewhere between 25–40 mm (see the temperature profiles in Fig. 3). Therefore, it seems that at axial positions higher than $Z = 25$ mm, entrainment of hot gases from an internal recirculation pattern into the TFB zone evaporates small droplets more rapidly than larger ones due to the d^2 evaporation law. Hence, for axial positions greater than 25 mm, SMD has its highest value near the inner boundary of the TFB zone due to the relative increase of large droplets in number. This trend of SMD profiles has been recognized as a characteristic of spray combustion having a hot central recirculation zone.[6] At $Z = 15$ and 25 mm, however, the maximum SMD points do not coincide with the maximum temperature ones. This feature of the SMD profiles at $Z = 15$ and 25 mm seems to occur since the temperature is not high enough to evaporate most small droplets, despite the maximum mean temperature being at the inner boundary of the TFB zone. Meanwhile, the maximum SMD value increases with an axial location up to $Z = 55$ mm. This trend is attributed to the continuous increase of the maximum mean temperature with axial position (see Fig. 3).

Drop Axial Velocity and Size PDFs

Figures 8a–8c exhibit the PDFs of drop axial velocities measured along three different drop-trajectories. These drop-trajectories are chosen at the radial position close to the inner (Fig. 8a) and outer (Fig. 8b) boundaries of the TFB zone and within the P/R zone (Fig. 8c). The notation 7.5/15-4 in Fig. 8 means radial and axial positions of 7.5 and 15 mm, respectively, marked by test point 4 in Figs. 3 and 7. The farthest radial position at which the effects of the internal recirculation zone is felt at each axial position was obtained by examination of the PDF of the drop axial velocities measured at different radial positions by Lee.[18] It is assumed that nonexistence of any section of the PDF curve in the negative velocity region and its symmetric shape can be interpreted as no or a minimal effect of the reversed-flow part of the gas recirculation zone on droplet flowfield.

Along a mean drop-trajectory near the inner boundary of the TFB zone in Fig. 8a, where maximum mean temperature occurs, one can clearly observe strong bimodal PDF up to an axial position of 25 mm. The left mode is in the negative axial velocity region indicating strong effects of central recirculation zone. It appears that this zone pulsates in time with its radial size changing in such a way to generate the bimodal drop velocity PDF shapes shown for $Z = 15$ and 25 mm in Fig. 8a, see also Edwards and Rudoff[8] and Edwards et al.[7] The size–velocity correlation indicates that most of the negative axial velocity drops are the small ones, easily affected by the pulsation. It is also interesting to note that along this drop-trajectory droplets on the average decelerate strongly and then accelerate moving away from the nozzle, see the mean velocity values in Fig. 8a.

Along a drop-trajectory within the TFB zone near its outer boundary in Fig. 8b the velocity PDF exhibits two different and distinct characteristics. Also, note that the strong left negative-drop-axial-velocity mode observed in Fig. 8a disappears. The mean axial drop velocity stays at about 10.5 m/s along the drop-trajectory. The shape of the PDF for positions at $Z = 15$ and 25 mm appears affected by the central recirculation zone. This is evidenced by extension of the left side of the PDF toward the negative values (skewed shape). However, the effect is not as strong as observed for the drop-trajectory near the inner boundary of the TFB zone. For $Z = 40$ and 55 mm the negative drop velocity portion of the PDF vanishes and shows a symmetric shape with low rms values.

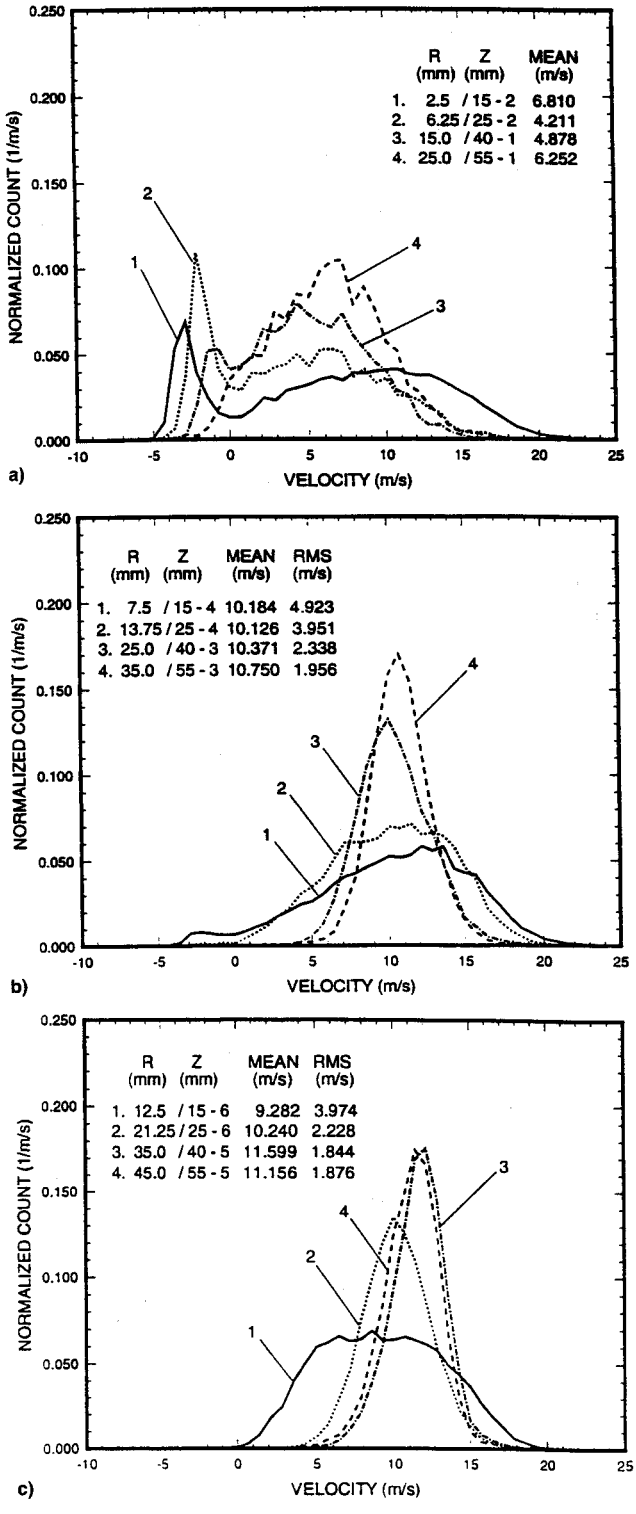

Fig. 8 PDF of the axial drop velocity along three mean drop trajectories close to a) inner and b) outer boundaries of the TFB zone and c) within the P/R zone.

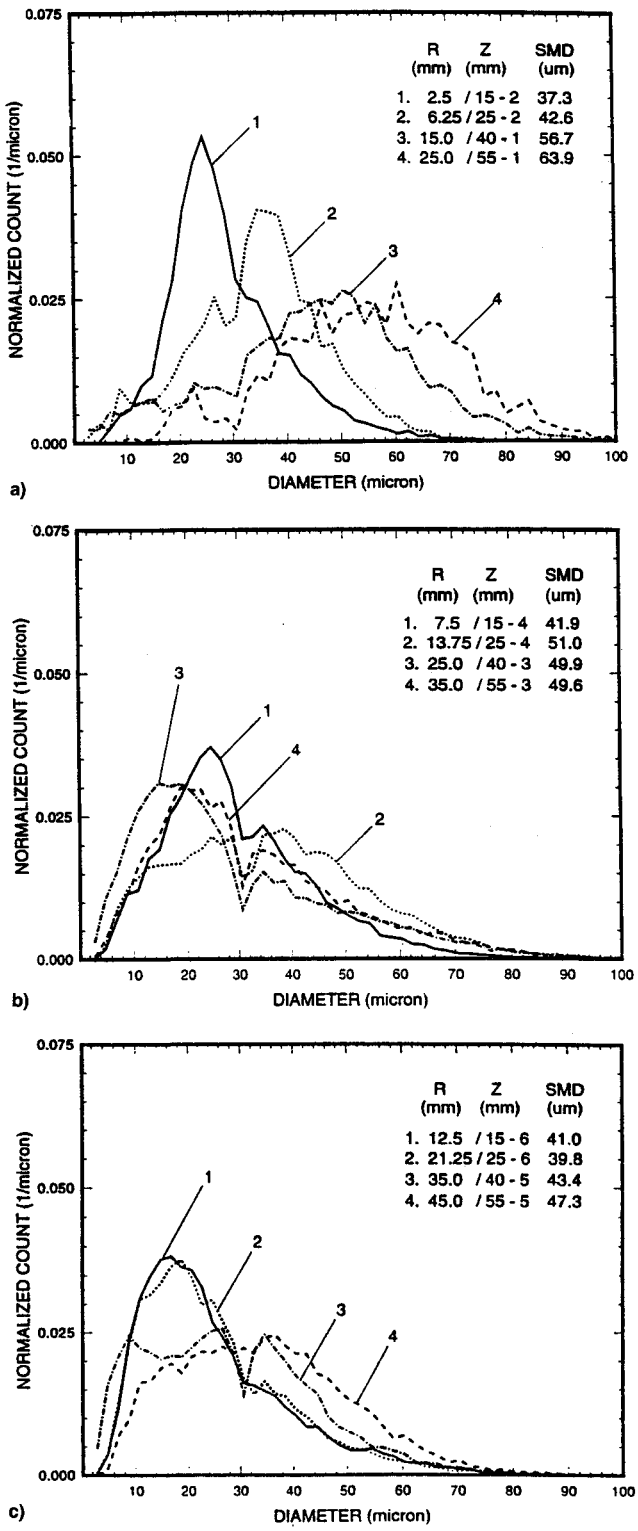

Fig. 9 PDF of the drop sizes along the same three mean drop trajectories as in Fig. 8.

Figure 8c is the PDF of axial drop velocity along a drop-trajectory within the P/R zone. Recirculation effects are only felt weakly at $Z = 15$ mm by extending the low drop axial velocity part of the PDF towards negative values. There is a mild acceleration along this drop-trajectory.

Figure 9a shows drop size PDF along the same drop-trajectory near the inner boundary of the TFB zone investigated in Fig. 8a. Note that the SMD consistently increases along this drop-trajectory. Being near the maximum mean temperature, the PDF plots suggest strong vaporization/burning of small droplets moving along this drop-trajectory. This is evidenced by a decrease in the number of small size droplets that proportionately cause an increase of the same for large drops. Rapid disappearance of small drops increases the significance of the large-diameter portion of the PDF so that they behave as shown in Fig. 9a. Note that the initial deceleration observed in axial drop velocity PDF also tends to increase the SMD of an ensemble of drops along the drop-trajectory. Examination of the size–velocity correlation by Lee[18] showed strong positive correlation, particularly for the

first two lower axial positions, hence, low velocity tail of the PDF is primarily caused by droplets of about less than 35–40 μm in size.

Along the same drop-trajectory within the TFB zone discussed in Fig. 8b, one can inspect the size PDF shown in Fig. 9b. Two important features are clear. First, PDFs are very near each other and the "PDF-shift" that was observed along the drop-trajectory near the inner boundary of the TFB zone in Fig. 9a is missing. SMD only increases from Z = 15 to 25 mm and stays nearly constant thereafter. This behavior is expected as the mean drop-trajectory is in the low mean temperature portion of the TFB zone (see Fig. 3). Second, the PDF has a valley in the neighborhood of the 30-μm drop size. In some cases (curves 2, 3, and 4) they suggest bimodal and in another (curve 1) just a minor dip. This effect is also weakly present along the drop-trajectory near the inner boundary of the TFB zone in Fig. 9a. Size–velocity correlation showed similar trends as for the earlier drop-trajectory with much weaker correlation for the 40- and 50-mm axial positions.

In Fig. 9c, along the same mean drop-trajectory within the P/R zone discussed before, SMD is nearly constant and PDFs have similar features mentioned for the drop-trajectory near the outer boundary of the TFB zone. Pulsation of the internal recirculation zone affects both the PDF of velocity and size. From Figs. 8 and 9 and the detailed high-radial-resolution measurements by Lee,[18] it appears that this pulsation strongly affects the velocity PDF only within the TFB zone and near its inner boundary. This is evidenced by the existence of a bimodal axial velocity PDF with one mode within the negative velocity region (strong effect) or by a negative velocity portion in the single-mode skewed PDF shape (weak effect). Detailed measurements by Lee and Fig. 9 show the peculiar valley shape close to the 30-μm drop size at nearly all axial positions (strongly) except at Z = 15 mm (weakly). The origin of this is unclear.

Conclusions

1) A mean spray flame structure and terminology are proposed from droplet flowfield measurements, flame photographs, and previous works in our engine laboratory that suggest P/R, TFB, and BG zones. Strong vaporization/burning of droplets are observed near the inner boundary of the TFB zone where (by definition) maximum mean temperature exists. In addition, an internal central recirculation also exists that pulsates in time.

2) The mean drop axial and radial velocities exhibit near-similar trends. They both increase monotonously from a minimum value at the inner boundary to a high and/or maximum value at the outer boundary of the TFB zone. The difference exists within the P/R zone where the axial component mildly decreases while the radial one increases with radial position. The mean tangential component is measured to be near-zero within the TFB zone, sharply increasing inside the P/R zone. In the TFB zone, therefore, the mean drop axial and radial velocity components mainly dominate the droplet flowfield in our spray.

3) Highest rms drop axial velocity is measured within the TFB zone with a decreasing trend towards the P/R zone. Lowest rms drop radial velocity occurs at the inner boundary of the TFB zone rising to a maximum near its outer boundary. The tangential rms drop velocities are the lowest of the three components and measure flat in shape within the TFB zone with a mild increase inside the P/R zone. Finally, it is clear that the droplet turbulence is not isotropic.

4) In a vertical plane passing through the combustor centerline, the mean drop velocity vector near the inner boundary of the TFB zone decreases in its magnitude from Z = 15 to 25 mm and then recovers its initial magnitude at Z = 55 mm, moving downstream along each drop-trajectory (deceleration/acceleration). This is due to the interaction of the droplet field with the core of the internal recirculation zone. However, the velocity vector near the outer boundary of the TFB zone maintains its initial magnitude downstream along any mean drop-trajectory. It appears that the mean drop-trajectory angle in spray combustion is established by and very near the angle at which the swirl flow enters the chamber with respect to the chamber centerline.

5) If the existence of an observable skewed or bimodal portion with negative drop axial velocity on the velocity PDF shape is viewed as indicative of the effect of the recirculation zone pulsation on droplets, then it appears that this effect is felt strongly within the entire TFB zone near the nozzle (Z = 15 and 25 mm). This effect diminishes in strength and primarily limits itself near the inner boundary of the TFB zone (Z = 40 and 55 mm). As one moves away from the nozzle, the size PDF along a trajectory near the inner boundary of the TFB zone (where maximum temperature occurs) shows a progressive decrease in the number of small drops due to vaporization and/or burning and, consequently, a proportionate relative magnification of the number of the large ones is detected. Away from this high-temperature trajectory, size PDFs are similar in shape and exhibit an unexplained feature near 30-μm size.

References

[1]Styles, A. C., and Chigier, N. A., "Combustion of Air Blast Atomized Spray Flames," *Sixteenth (International) Symposium on Combustion*, The Combustion Inst., Pittsburgh, PA, 1977, pp. 616–630.

[2]Mao, C. P., Wang, G., and Chigier, N., "An Experimental Study of Air-Atomizer Spray Flames," *Twenty-First (International) Symposium on Combustion*, The Combustion Inst., Pittsburgh, PA, 1986, pp. 665–673.

[3]Heitor, M. V., and Whitelaw, J. H., "Velocity, Temperature, and Species Characteristics of the Flow in a Gas Turbine Combustor," *Combustion and Flame*, Vol. 64, 1986, pp. 1–32.

[4]Presser, C., Gupta, A. K., and Semerjian, H. G., "Droplet Velocity Measurements in a Swirling Kerosene Spray Flame," American Society of Mechanical Engineers Winter Annual Meeting, San Francisco, CA, 1986.

[5]Presser, C., Gupta, A. K., and Semerjian, H. G., "Droplet/Air Interaction in Swirl-Stabilized Spray Flame," *2nd ASME/JSME Joint Thermal Engineering Conference* (Honolulu, HI), 1987, pp. 73–83.

[6]Edwards, C. F., Rudoff, R. C., and Bachalo, W. D., "Phase Doppler Anemometer Measurements of a Swirl-Stabilized Kerosene Spray Flame," ILASS-America, 4th Annual Conf. on Liquid Atomization and Spray Systems, 1990.

[7]Edwards, C. F., Rudoff, R. C., and Bachalo, W. D., "Measurement of Correlated Droplet Size and Velocity Statistics, Size Distribution, and Volume Flux in a Steady Spray Flame," Fifth International Symposium on the Applications of Laser Technique to Fluid Mechanics, Lisbon, Portugal, 1990.

[8]Edwards, C. F., and Rudoff, R. C., "Structure of Swirl-Stabilized Spray Flame by Imaging, Laser Doppler Velocimetry, and Phase Doppler Anemometry," *Twenty-Third (International) Symposium on Combustion*, The Combustion Inst., Pittsburgh, PA, 1990, pp. 40–55.

[9]Bicen, A. F., Tse, D. G. N., and Whitelaw, J. H., "Combustion Characteristics of a Model Can-Type Combustor," *Combustion and Flame*, Vol. 80, 1990, pp. 111–125.

[10]Costa, M., Costen, P., and Lockwood, F. C., Combustion Science and Technology, Vol. 75, 1991, pp. 129–154.

[11]McDonell, V. G., and Samuelsen, G. S., "Gas and Drop Behavior in Reacting and Nonreacting Air-Blast Atomizer Sprays," *Journal of Propulsion and Power*, Vol. 7, 1991, pp. 684–691.

[12]Presser, C., Gupta, A. K., and Semerjian, H. G., "Aerodynamic Characteristics of Swirling Kerosene Spray Flame: Pressure-Jet Atomizer," *Combustion and Flame*, Vol. 92, 1993, pp. 25–44.

[13]Gupta, A. K., Lilly, D. G., and Syred, N., "Swirl Flow," Abacus Press, Cambridge, MA, 1984.

[14]Bachalo, W. D., "Method for Measuring the Size and Velocity of Spheres by Dual-Beam Light-Scatter Interferometry," *Applied Optics*, Vol. 19, No. 3, 1980, p. 120.

[15]Chehroudi, B., and Ghaffarpour, M., "Spray Drop Size and Velocity Measurements in a Swirl-Stabilized Combustor," 36th American Society of Mechanical Engineers International Gas Tur-

bine and Aeroengine Congress and Exposition, Paper 91-GT-43, Orlando, FL, 1991.

[16]Chehroudi, B., and Ghaffarpour, M., "Structure of Hollow-Cone Spray with and Without Combustion," 37th American Society of Mechanical Engineers International Gas Turbine and Aeroengine Congress and Exposition, Paper 92-GT-124, Koln Mess Cologne, Germany, 1992.

[17]Ghaffarpour, M., and Chehroudi, B., "Experiments on Spray Combustion in a Gas Turbine Model Combustor," *Combustion Science and Technology*, Vol. 92, 1993, pp. 173–200.

[18]Lee, K., "Structure of a Swirl-Stabilized Spray Flame by Drop Size and Three-Component Velocity Measurements," M.S. Thesis, Dept. of Mechanical Engineering, Univ. of Illinois at Chicago, IL, 1993.

[19]Khalil, E. E., El-Mahallaway, F. M., and Moneib, H. A., "Effects of Combustion Air Swirl on the Flow Pattern in a Cylindrical Oil Fired Furnace," *Sixteenth (International) Symposium on Combustion*, The Combustion Inst., Pittsburgh, PA, 1977, pp. 135–143.

[20]Shi, R. X., and Chehroudi, B., "Velocity Characteristics of a Confined Highly-Turbulent Swirling Flow near a Swirl Plate," *Journal of Fluids Engineering*, Vol. 116, 1994, pp. 685–693.

[21]Chehroudi, B., and Ghaffarpour, M., "Anatomy of an Isothermal and Burning Hollow-Cone Spray," *Atomization and Sprays* (to be published).

[22]Chehroudi, B., "Preliminary Drop Size and Velocity Measurements in a Dense Diesel-Type Spray," SAE International Off-Highway and Powerplant Congress and Exposition, Society of Automotive Engineers Paper 901673, Milwaukee, WI, 1990.

[23]Bachalo, W. D., Rudoff, R. C., and Brena de la Rosa, A., "Mass Flux Measurements of a High Number Density Spray System Using the Phase Doppler Particle Analyzer," AIAA Paper 88-02636, 1988.

[24]McDonell, V. G., and Samuelsen, G. S., *Sensitivity Assessment of a Phase Doppler Interferometer to User-Controlled Setting, Liquid Particle Size Measurement Techniques: 2nd Volume*, edited by E. D. Hirleman, W. D. Bachalo, and P. G. Felton, American Society of Testing and Materials, ASTM STP 1083, Philadelphia, PA, 1990, pp. 170–189.

[25]Presser, C., Gupta, A. K., Avedisian, C. T., and Semerjian, H. G., "Effect of Dedecanol Content on the Combustion of Methanol Spray Flames," *Proceedings of the 5th International Conference on Liquid Atomization and Spray Systems* (Gaithersburg, MD), 1991, pp. 521–528.

[26]Durst, F., Melling, A., and Whitelaw, J. H., *Principles and Practice of Laser-Doppler Anemometry*, 2nd ed., Academic, New York, 1981.